Breast Cancer Res Treat (2014) 145:45–59
DOI 10.1007/s10549-014-2940-8

PRECLINICAL STUDY

Discovery of structure-based small molecular inhibitor of αB-crystallin against basal-like/triple-negative breast cancer development in vitro and in vivo

Zhijuan Chen · Qing Ruan · Song Han · Lei Xi · Wenguo Jiang · Huabei Jiang · David A. Ostrov · Jun Cai

Received: 10 January 2014 / Accepted: 26 March 2014 / Published online: 8 April 2014

Abstract αB-crystallin (CRYAB) is present at a high frequency in poor prognosis basal-like breast tumours, which are largely absent of oestrogen, progesterone receptors and HER2 known as triple-negative breast cancer (TNBC). CRYAB functions as a molecular chaperone to bind to and correct intracellular misfolded/unfolded proteins such as vascular endothelial growth factor (VEGF), preventing non-specific protein aggregations under the influence of the tumour microenvironment stress and/or anti-cancer treatments including bevacizumab therapy. Directly targeting CRYAB can sensitize tumour cells to chemotherapeutic agents and decrease tumour aggressiveness. However, growing evidence shows that CRYAB is a critical adaptive response element after ischemic heart disease and stroke, implying that directly targeting CRYAB might cause serious unwanted side effects. Here, we used structure-based molecular docking of CRYAB and identified a potent small molecular inhibitor, NCI-41356, which can strongly block the interaction between CRYAB and $VEGF_{165}$ without affecting CRYAB levels. The disruption of the interaction between CRYAB and $VEGF_{165}$ elicits in vitro anti-tumour cell proliferation and invasive effects through the down-regulation of VEGF signalling in the breast cancer cells. The observed in vitro anti-tumour angiogenesis of endothelial cells might be attributed to the down-regulation of paracrine VEGF signalling in the breast cancer cells after treatment with NCI-41356. Intraperitoneal injection of NCI-41356 greatly inhibits the tumour growth and vasculature development in in vivo human breast cancer xenograft models. Our findings provide 'proof-of-concept' for the development of highly specific structure-based alternative targeted therapy for the prevention and/or treatment of TNBC.

Keywords CRYAB · $VEGF_{165}$ · Small molecular inhibitor · TNBC

Abbreviations

TNBC	Triple-negative breast cancer
CRYAB	αB-crystallin
VEGF	Vascular endothelial growth factor
ER	Oestrogen receptor
PG	Progesterone receptor
HER2	Human EGF (epidermal growth factor) receptor 2

Electronic supplementary material The online version of this article (doi:10.1007/s10549-014-2940-8) contains supplementary material, which is available to authorized users.

Z. Chen · Q. Ruan · J. Cai
Department of Anatomy and Cell Biology, University of Florida, 1600 SW Archer Road, Gainesville, FL, USA

S. Han
Department of Surgery, University of Florida, 1600 SW Archer Road, Gainesville, FL, USA

L. Xi · H. Jiang
Department of Biomedical Engineering, University of Florida, 1600 SW Archer Road, Gainesville, FL, USA

W. Jiang · J. Cai (✉)
Cardiff University-Peking University Cancer Institute, Institute of Cancer & Genetics, Cardiff University, Heath Park, Cardiff, UK
e-mail: caiJ5@cardiff.ac.uk; jucai@ufl.edu

D. A. Ostrov
Department of Pathology, Immunology and Laboratory Medicine, University of Florida, 1600 SW Archer Road, Gainesville, FL, USA

Introduction

Invasive breast cancer affects more than 1.3 million women worldwide each year, and accounts for around 15 % of female cancer-related deaths. The incidence of breast cancer has increased over the past 10 years and remains a considerable health burden despite significant advances in treatment of oestrogen receptor (ER) positive disease in particular [1]. The development of gene array profiling has allowed for the classification of breast cancer into several subtypes based on distinctive gene expression signatures, including basal-like breast cancer showing high expressions of characteristic basal epithelial proteins (basal markers) [2]. Most basal-like breast cancers do not express ER, progesterone receptor (PG) and HER2 [3]. Since the hormone receptors and HER2 are central to the biologic variance among breast cancers, clinicians tend to categorize triple-negative breast cancer (TNBC) by routine immunohistochemical staining, as a surrogate profiling for the basal-like breast cancer in the clinical settings [4]. Clinical surveys reveal that approximately 15 % of all breast cancers are diagnosed as TNBC, occurring more frequently among younger women (<40 years old) with a high histological grade, risk of recurrence, worse disease prognosis and disease-free survival [5–9].

Treatment of TNBC is particularly problematic, with cytotoxic chemotherapy remaining the standard course of treatment despite lack of long-term effectiveness. Many studies have demonstrated that enhanced angiogenesis supports rapid growth and early metastases in patients with TNBCs [10, 11]. The primary and best-characterized mediator of tumour angiogenesis is vascular endothelial growth factor (VEGF). However, recent investigations into the use of bevacizumab (Avastin®) (a humanized anti-VEGF monoclonal antibody) alongside chemotherapy have ultimately proved disappointing [12, 13]. Despite the improvement in response rate (RR) and progression-free survival (PFS), a significant fraction of patients on this combination therapy proved to be non-responsive. Even to the most responsive patient, initial response (tumour static or shrinkage) to bevacizumab therapy was followed almost inevitably by tumour re-growth, indicative of resistance to bevacizumab. Apart from classical paracrine and autocrine patterns, the internal autocrine (intracrine) VEGF signalling is critical for cell homeostasis. For instance, it has been shown that serious vascular defects occur in animals devoid of intracrine VEGF signalling, which could not be rescued by exogenous VEGF [14]. With the help of the intracrine VEGF signalling, both cancer cells and associated endothelial cells might be able to escape from the blocking exogenous VEGF such as bevacizumab treatment [15].

αB-crystallin (CRYAB) is one of the commonly characteristic 'basal markers' of TNBC closely correlated with the poor prognosis of TNBC [16, 17]. CRYAB was first discovered in vertebrate lens and is responsible for maintaining the lens transparency [18]. However, subsequent studies revealed that CRYAB can be induced by cellular stress as a bona-fide small heat shock protein (HspB5) in other non-lenticular tissues [19]. Recent confirmation of significantly increased CRYAB expression (Q-PCR analysis) in invasive breast cancer tissues has been reported by our group [20]. A high correlation has been found between CRYAB expression and clinical parameters such as tumour stage, metastasis status, histological grade and ER status. CRYAB functions as a molecular chaperone, preventing non-specific protein interactions during cellular stress, a driving force behind adaptations to harmful tumour microenvironments such as hypoxia, acidosis, nutrient deprivation and host immune insults [21]. CRYAB also plays a role in the inhibition of apoptosis in response to diverse stimuli. Moreover, direct targeting of CRYAB using anti-sense or RNAi molecules has been shown to sensitize tumour cells to chemotherapeutic agents and apoptosis inducers [22].

Previous studies by our group showed that CRYAB binds to and corrects the unfolded/misfolded VEGF under cellular stress of the tumour microenvironment and/or anti-VEGF treatment [20]. As a result, CRYAB has been proposed as a target for TNBC treatment, which may lead to down-regulation of intracrine VEGF signalling. However, growing evidence reveals that CRYAB is a critical adaptive response element of cardioprotection mechanisms in cardiomyocytes and microvascular endothelial cells during ischaemic heart disease [23]. The protective role of CRYAB has also been reported in damages to the central nervous system (CNV) by modulating the immune system [24]. In this study, we developed a novel strategy to target CRYAB for the therapy of TNBC by disrupting the interaction between CRYAB and VEGF, which could avoid unwanted side effects of directly targeting CRYAB, and thus serve as a potential new targeted therapy for TNBC.

Materials and methods

Molecular docking

We used the α-crystallin domain (ACD) crystal structure of human CRYAB as the basis for molecular docking simulation. Sequence studies showed that the ACD of CRYAB is preceded by an N-terminal region, containing β strands (β3, β7, β8 and β9) and helical sequences with the strongest interactions with many growth factors including $VEGF_{165}$ [25]. Our inhibitory competition study using the

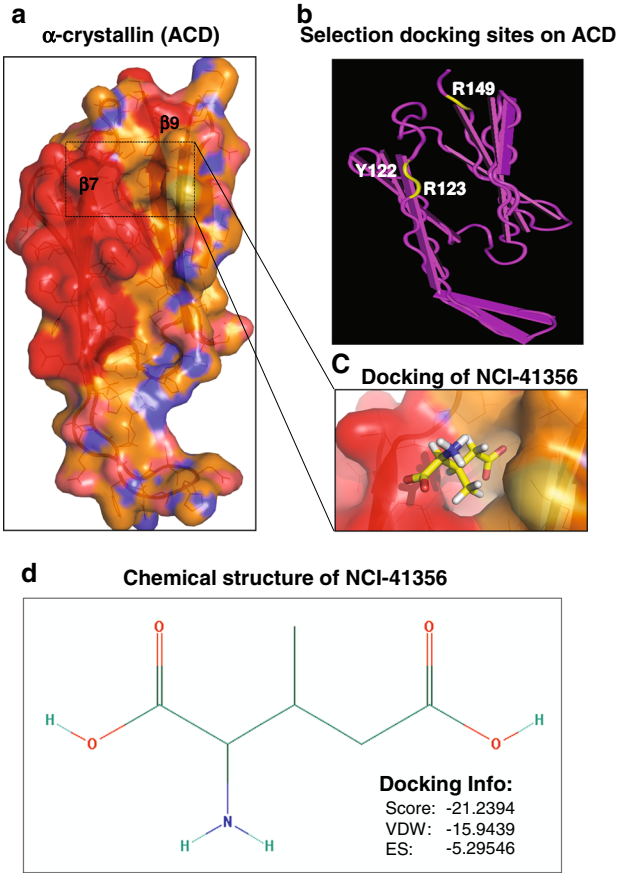

Fig. 1 Molecular docking of CRYAB. **a** Molecular surface of CRYAB (*orange* for carbon, *blue* for nitrogen, *pink* for oxygen) indicating the potential sites for docking (*red*). **b** The residues that are essential for $VEGF_{165}$ binding to the ACD of CRYAB. **c** Small molecular compound NCI-41356 is shown as posed by molecular docking to the ACD of CRYAB, exhibiting a high molecular score of −21.2 DOCK units. **d** The chemical structure of NCI-41356

decoy peptides corresponding to CRYAB with $VEGF_{165}$ demonstrated that β7 and β9 play the most crucial role in the interaction between CRYAB and $VEGF_{165}$ (Supplementary Fig. 1). We then selected a structural pocket which includes amino acid residues Y122/R123/R149 of human CRYAB (Fig. 1a, b). To prepare the sites for docking, all water molecules were removed. We defined the sites for molecular docking using SPHGEN, a programme with the ability to generate an unbiased grid of points that reflect the actual surface of the selected sites. Docking calculations were carried out with DOCK6.5 (UCSF). A file containing the atomic coordinates of 139,735 small molecular compounds in a repository at the National Cancer Institute Development Therapeutics Program (http://dtp.nci.nih.gov/branches/npb/repository.html) was obtained from ZINC (UCSF). Grid-based scoring was used by DOCK6.5 run by parallel processing at the University Florida High Performance Computing Facility.

PathHunter™ cell-based CRYAB/$VEGF_{165}$ interaction assay

DiscoveRX has developed a custom cell-based assay to monitor the interaction of CRYAB and a cytosolically localized $VEGF_{165}$ with signal sequence removed. The two candidate proteins were fused to β-galactosidase (β-Gal) complementation fragments. CRYAB was co-expressed with a larger sequence encoding a majority of β-Gal [enzyme acceptor (EA)], while $VEGF_{165}$ was fused to a small peptide epitope of β-Gal [Prolink (PK)]. The two separated β-Gal fragments are inactive. After the constructs are transduced into U2OS cells, interaction of the fused CRYAB and $VEGF_{165}$ can result in recombined active β-Gal. In theory, disruption of the interaction between CRYAB and $VEGF_{165}$ is quantified by measuring the amount of active β-Gal through its conversion of a nonluminescent substrate to a luminescent product (Supplementary Fig. 2). On the day before the experiment, the U2OS cells were briefly thawed in a 37 °C water bath between 10 s and 1 min until only small icy crystals remained and transferred to pre-warmed PathHunter® Cell plating 0 reagent (cat#93-0563R0A; DiscoveRX). The cells were counted and 20 µl of the cell suspension transferred to each well of a 384-well white-walled, clear bottom plate (cat#3707; Corning Life Sciences) at the indicated cell densities. Seeded cells were incubated for 24 h at 37 °C and in 5 % CO_2. The small molecular compounds dissolved in vehicle (0.1 % DMSO), and 5 µl per well of the compounds were added to the cells. After incubating for 90 min at 37 °C and in 5 % CO_2, 12 µl per well of PathHunter Detection Reagents (cat#93-001; DiscoveRX) were added and the plates were incubated for 60 min at room temperature. The plates were read using the POLARstar imaging system (BMG).

Cell culture

Breast cancer cell lines including original MDA-MB-231 and MDA-MB-436 were obtained from the American Type Culture Collection (ATCC) and maintained in Delbecco's Modified Eagle's Media (DMEM) supplemented with 10 % FCS. Highly malignant breast cancer cells were developed by three in vivo passages of the parental breast cancer cells in athymic nude mice (Supplementary method and Supplementary Fig. 3a). Human microvascular endothelial cells (HMECs) were purchased from the Life Technologies and maintained in microvascular endothelial cell basal medium with growth supplement (Life Technologies) at 37 °C in 5 % CO_2. HMECs were used between passage 1 and 3. Cell lines were passaged for less than

6 months, and no further authentication was done on these cell lines.

VEGF ELISA measurement

Endogenous $VEGF_{165}$ production and secretion from the cells were assayed using RayBio® human VEGF ELISA (RayBiotech, Inc.) and human VEGF DuoSet ELISA (R&D system) according to the manufacturers' instructions, respectively. Breast cancer cells were grown to 80 % confluence in 6-well plates at 1×10^5 cells/well. In order to block de novo protein synthesis, the cells were incubated with 60 μg/ml cycloheximide for 1–1.5 h before treatment. Prior to cell counting, the supernatant was harvested by centrifugation at 2,000×*g* for 10 min, while the cell lysates were prepared as described [26]. $VEGF_{165}$ concentrations were measured in duplicate in each sample. The results were expressed as $VEGF_{165}$ (pg) per 10^6 cells in at least three separate experiments.

Breast tumour cell proliferation curve

Crystal violet assays were conducted to quantify breast cancer cell proliferation as previously described [26]. Briefly, the cells were seeded onto 24-well plates at 1×10^5 cell/ml. The medium was replaced every three days. After the indicated treatment intervals, the cells were fixed in 4 % paraformaldehyde in PBS for 15 min. After washing with distilled water, the plates were stained with 0.1 % crystal violet solution for 20 min. The plates were thoroughly washed with water and allowed to dry. 100 μl of 33 % acetic acid was added to each well for extraction of the dye. Absorbance of the staining was measured using an automatic microtiter plate reader at 590 nm.

Breast tumour cell motility analysis

The motility of breast cancer cells was analysed using a wound-healing assay. The cells were grown in 24 well-plates until they reached confluence. To prevent cell proliferation at the wound edge, the cell monolayers were treated with 25 mg/ml 5-fluorouracil for 5 min followed by 2.5 mm scrapes in the cell monolayers were made in one direction. The wounded cell monolayers were washed with PBS to remove cell debris and subjected to the indicated treatments for 6 h. The migration of the invading cell front was monitored and photographed at initial wounding (0 h) and at 6 h under a phase-contrast microscope equipped with a digital camera. Cell migration was calculated as the distance (μm) migrated into the wound area = (the distance between the two wound edge at 0 h − the distance at 6 h)/2.

In vitro analysis of the effects of breast tumour cells co-cultured with microvascular endothelial cells

An in vitro co-culture system was employed as previously described [20]. For measuring endothelial cell proliferation, MDA-MB-231 cells were seeded onto 24-well Transwell inserts with 0.4 μm pores (Corning Life Sciences) with the indicated treatments. Human microvascular endothelial cells (HMECs) (Life Technologies) were cultured in the low chambers of the same 24-well plates. After 24 h, HMECs were fixed and subjected to crystal violet staining as described above. In sets of in vitro tubule formation assays, HMECs (2.5×10^4/well) were seeded between two layers of 12.5 % Matrigels (BD) at the lower chambers of the 24-well plates in which the MDA-MB-231 cell-seeded Transwell inserts were placed. The following day, the HMEC cultures were observed under a phase-contrast microscope and photographed at random in five fields (×10). The tubule length (mm/mm^2) per microscopic filed was quantified.

Mice breast cancer xenograft models

All animals used in this study were maintained at the animal facility of the University of Florida and handled in accordance with the institutional guidelines. Athymic female nude mice (*nu/nu*) aged 5–8 weeks were purchased from Charles River Laboratories (Charles River Laboratories) and caged in groups of 5 or fewer. The third in vivo passaged MDA-MB-231 cells were harvested, and a single cell suspension with >95 % viability (1×10^5) was injected subcutaneously into the mammary fat pads of the mice. Tumour volumes were determined by calliper measurements of the large (*a*) and smallest (*b*) diameters of each tumour using formula $a \times b^2 \times 0.4$ in a blinded manner. After the tumours were established ($\sim$30 mm^3 in size 4 days after tumour cell implantation), the mice were randomly assigned to receive treatments of vehicle or compound (NCI-41356). The maximum tolerated dose of NCI-41356 was determined (Supplementary methods). Even though all three tested doses (0.2, 0.4 and 0.8 g/kg) of NCI-41356 were well tolerated as the change of bodyweight being within 10 %, only the dosing regimen of 0.2 g/kg did not cause weight loss (Supplementary Fig. 3b). As shown in Supplementary Fig. 3a, in vivo passaged MDA-MD-231 cells exhibited the ability to rapidly grow to $\sim$700 mm^3 within 2 weeks. However, 1.2 cm of diameter (equivalent to $\sim$700 mm^3) is the maximum size that the tumours are allowed to attain under institutional guideline of the University Florida. As a result, we decided that 0.2 g/kg NCI-41356 was administrated via intraperitoneal injection (i.p.) every two days for 8 consecutive days. Mice were anaesthetized with a mixture of ketamine (85 mg/kg)/xylazine (4 mg/kg) during the tumour

implantation and i.p. injection of the small molecular compound. All mice were euthanized when the tumour volume in the vehicle-treated group reached ~ 300 mm^3.

Noninvasively monitoring of in vivo tumour growth and tumour angiogenesis

We used an acoustic-resolution photoacoustic microscopy (ARPAM) system to monitor tumour development and tumour vascular change in breast cancer xenograft mice as previously described [27]. During longitudinal photoacoustic (PA) imaging (20 min/each time), mice were kept anaesthetized with a mixture of ketamine (85 mg/kg)/xylazine (4 mg/kg), and their body temperatures were maintained at 37 °C by a temperature controlling pad. Mice skin at the tumour inoculation sites was gently depilated before tight contacting with the membrane-sealed imaging window in the bottom of the water tank, and the gap was filled with ultrasound gel serving as matching medium for PA signals. The two-dimensional transverse scanning combined with the depth-resolved ultrasonic detection generated 3D PA images displayed in maximum amplitude projection (MAP). 3D PA signals were processed by Hilbert transform [28] and the data normalized to the same scale (0–256) with a threshold (−6 dB level). Entropy was calculated from normalized MAP of each PA image at the same scale (0–256). The volumes of the blood vessels were calculated by integrating the corresponding image voxels (1 for blood vessel and background being set to 0).

Statistical analysis

Experiments were performed at least three times. The statistical significance between experimental and control groups was determined by the unpaired Student *t*-test, including cell-based interaction assay, ELISA measurement, crystal violet staining, wound-healing assay, in vitro tubule formation, as well as in vivo animal experiments such as tumour volume, entropy and normalized vessel volume. Results are expressed as mean ± SEM. Statistical analysis was performed using GraphPad Prism (version 5.01; GraphPad Software, Inc.) with $p < 0.05$ considered statistically significant.

Results

Analysis of the interaction between CRYAB and $VEGF_{165}$

CRYAB is a member of the small heat shock proteins (sHsps) family. Sequence analysis reveals that all sHsps contain a conserved ACD followed by a variable N-terminal region [29]. Of the six $VEGF_{165}$ interactive sequences identified by protein pin arrays in human CRYAB, five are located within the conserved ACD. Chaperone assays confirm that CRYAB protects $VEGF_{165}$ from unfolding and aggregation through these surface interactive sequences [25].

In order to obtain better understanding whether these interactive sequences offer the most appealing hotspots to human CRYAB binding to $VEGF_{165}$, we designed five decoy peptides (*49/56, *91/98, *117/124, *143/150 and *157/164) corresponding to the five sequences of $VEGF_{165}$ interacting regions of human CRYAB ($_{49}$LRPPSFLR$_{56}$, $_{91}$VKVLGDVI$_{98}$, $_{117}$EFHRKYRI$_{124}$, $_{143}$TVNGPRK$_{150}$ and $_{157}$RTIPTRE$_{164}$) and a control 'scrambled' (*scr) peptide with the same amino composition of *157/164 (Supplementary Fig. 1a). The *scr peptide sequence did not show significant homology to any known protein motifs, as determined by a motif mining algorithm (http://www.motif.genome.ad.jp/; data not shown). To facilitate translocation of the decoy peptides into cultured cells, the amino terminus of each peptide was tagged with the 16 amino acid penetratin sequence derived from the third helix of the *Drosophila melanogaster* antennapedia homeodomain protein [30].

In order to characterize whether the decoy peptides affect the interaction between CRYAB and $VEGF_{165}$, we employed a customized PathHunter^{TM} cell-based CRYAB/$VEGF_{165}$ interaction assay (DiscoveRX) (Supplementary Fig. 2a). Employing this system in U2OS cells, we observed that only *117/124 and *143/150 resulted in a significant reduction of the interaction between CRYAB and $VEGF_{165}$ in a dose-dependent manner, while the other decoy peptides including *scr did not exert a detectable disruptive effect on the interaction between CRYAB and $VEGF_{165}$ (Supplementary Fig. 1b). This suggested that both $VEGF_{165}$ interacting regions ($_{117}$EFHRKYRI$_{124}$, $_{143}$TVNGPRK$_{150}$) might contain key residues (hotspots) contributing to the interaction between CRYAB and $VEGF_{165}$. To ensure that the effects of the decoy peptides were not influenced by differential internalization efficiencies, we evaluated the uptake of fluoresceinated (FITC-) *49/56, *91/98, *117/124, *143/150, *157/164 and *scr by U2OS cells using confocal microscopy and flow cytometry. Direct fluorescence imaging showed that all six decoy peptides were efficiently internalized into the U2OS cells, which was further confirmed by flow cytometry data (Supplementary Fig. 1c).

Molecular docking and identification of small molecular compounds inhibiting the interaction between CRYAB and $VEGF_{165}$

Molecular insight into ACD is obtained from the studies of crystal structures of the other sHsp oligomers including

Methanococcus jannaschii (Mj) Hsp16.5, *Triticum aestivum* (Ta) Hsp16.9 and *Taenia saginata* (Tsp) 36, suggesting that ACD is a β-sandwich containing β2–β9 strands. Recently, a solid-/solution-state NMR study of ACD and full-length human CRYAB showed that the β3–β7–β9 groove appears to be a common surface that mediates interactions of CRYAB with multiple proteins, including $VEGF_{165}$ [31]. This notable structural feature which is formed in part by $_{117}EFHRKYRI_{124}$ and $_{143}TVNGPRK_{150}$ contains β7 and β9 strands, respectively (Fig. 1a). After careful evaluation, we selected the structural pocket formed by discontinuous segments from β7 and β9 strands containing amino acids Y122/R123/R149 as putative binding sites for the basis of molecular docking small molecular compounds (Fig. 1b). We used molecular docking to simulate the interaction of 139,735 small molecular compounds (from the NCI Developmental Therapeutics Program) with the selected structural pocket on the crystal structure of ACD. The small molecular compounds were ranked based on their overall energy scores (taking into account polar and nonpolar interactions between the small molecules and the protein), and the 40 highest scoring compounds were requested for functional evaluation (Table 1).

Efficient small molecular compounds disrupting the interaction between CRYAB and $VEGF_{165}$

For initial screening, we selected the MTT assay to identify small molecular compounds that reduce the viability of highly malignant TNBC cells including MDA-MB-231 and MDA-MB-436. Although many reports suggested that parental MDA-MB-231 cells express very little CRYAB [32], we found that our in vivo passaging method (Supplementary methods and Supplementary Fig. 3a) has dramatically enhanced CRYAB expression in MDA-MB-231 (Supplementary Fig. 3c). Furthermore, the brain metastasis-derived MDA-MB-231 (MDA-MB-231-BR) cells exhibited highest expression of CRYAB, whereas CRYAB was not detected in MCF-7 cells. It was our hope that this approach would allow us to identify small molecular compounds inhibiting breast tumour formation. The dose–response curve for the inhibition of breast cancer cells showed that only four compounds significantly reduced the viability of the breast cancer cells (Supplementary Table 1).

Given that the four small molecular compounds were identified in the initial screening, we next determined whether these small molecular molecules disrupted the interaction between CRYAB and $VEGF_{165}$. The PathHunter™ cell-based CRYAB/$VEGF_{165}$ interaction assays revealed that the NCI-41356 (Fig. 1c, d) significantly reduced the interaction between CRYAB and $VEGF_{165}$ in a dose-dependent manner (Fig. 2a). Full name for NCI-41356 is (2S,3R)-3-methylglutamic acid hydrochloride salt. NCI-41356 displayed a twofold inhibition response at 20,000 cells/wells and a 1.5-fold window using 5,000 cells/well at the highest concentration (100 μM). However, we observed no significant inhibitory effects with the other three leading small molecular compounds (Supplementary Fig. 2b).

Disruption of the interaction between CRYAB and $VEGF_{165}$ affects VEGF in breast cancer cells

One of the important mechanisms by which CRYAB contributes to tumour development is through up-regulation of VEGF and maintenance of VEGF signalling. Our previous study indicated that CRYAB might bind to and prevent misfolded/unfolded $VEGF_{165}$ from proteolytic degradation [33]. We reasoned that the VEGF production in breast cancer cells could be affected by the disruption of the interaction between CRYAB and $VEGF_{165}$. Both $VEGF_{165}$ concentrations of the cell lysates and supernatants were measured by ELISA assays (Fig. 2b). A substantial decrease in $VEGF_{165}$ expression was detected in both breast cancer cell lines (MDA-MB-231 and MDA-MB-436) treated with NCI-41356 (≥25 μM). The level of supernatant soluble $VEGF_{165}$ was ~300 pg/ml (in 1×10^6 cells) in both breast cancer cells (MDA-MB-231 and MDA-MB-436) treated with 100 μM NCI-41356, representing a 40 % decrease from the $VEGF_{165}$ level of ~700 pg/ml (in 1×10^6 cells) in those received vehicle treatment. In addition, NCI-41356 (100 μM) reduced cell lysate $VEGF_{165}$ level from ~100 pg/ml (in 1×10^6 cells) to ~60 pg/ml (in 1×10^6 cells) in both breast cancer cells (MDA-MB-321 and MDA-MB-436) treated with vehicle. This represented a ~40 % decrease. These observations support a new paradigm in which the disruption of the interaction between CRYAB and $VEGF_{165}$ can lead to inhibition of VEGF production in tumour cells.

Disruption of the interaction between CRYAB and $VEGF_{165}$ decreases the malignant behaviour of breast tumour cells

The effects of various concentrations of NCI-41356 on cell viability were assessed by crystal violet assays. The inhibitory effect of NCI-41356 was time-dependent with a much greater effect observed on the prolonged treatments. In Fig. 3a, the greatest inhibitory effect of NCI-41356 on both MDA-MB-231 and MDA-MB-436 cell proliferation was reached at 100 μM after a 7-day treatment. At low doses (<10 μM), no effects were seen compared with the vehicle treatment. The effects of NCI-41356 (10–50 μM)

Table 1 Molecular docking scores of SMIs selected by interactions with a structural pocket of CRYAB at and around amino acid residues Y59/R60/R86

ZINC#	NCI#	M.W.	Energy score	VDW score	ES score
01870301	129468	247.1007	−24.1690292358398	−15.6160125732421	−8.55301570892333
01610745	6080071	238.0731	−23.7817726135253	−13.4533605575561	−10.3284111022949
01574931	89296	199.0999	−23.4884643554687	−15.4158267974853	−8.07263755798339
1587797	1042	161.1572	−23.0438518524169	−17.7066783905029	−5.3371729850769
05395789	282051	178.1654	−23.0107383728027	−18.3419818878173	−4.6687569618225
01870312	129478	247.1007	−22.8254814147949	−17.8408260345458	−4.98465490341186
05215284	220235	155.1252	−22.6773777008056	−11.9523487091064	−10.7250289916992
01701052	108912	191.2014	−22.103229522705	−18.7663650512695	−3.33686399459838
01595538	403251	211.1306	−21.572395324707	−17.3273200988769	−4.24507617950439
01647421	679063	211.1366	−21.4023838043212	−19.4118900299072	−1.99049401283264
01672629	41356	161.1572	−21.2394008636474	−15.94393825531	−5.29546213150024
01711849	122445	170.0842	−21.0939331054687	−18.2374877929687	−2.85644388198852
01635542	163127	181.5755	−21.0245475769042	−19.393627166748	−1.63092100620269
04782975	36592	203.1542	−20.6739425659179	−18.2918968200683	−2.38204598426818
03953973	40837	190.0291	−20.6354293823242	−14.9605998992919	−5.67482995986938
01693057	65880	188.1195	−20.6216087341308	−16.0131130218505	−4.60849523544311
01700536	108368	180.1598	−20.5869522094726	−17.3973217010498	−3.18963098526
01587602	805	200.1044	−20.5175819396972	−16.8287506103515	−3.68883109092712
01605843	525117	180.5937	−20.4932231903076	−19.9514350891113	−0.541787028312683
00208097	402845	218.1684	−20.4700298309326	−18.0754241943359	−2.39460611343383
01750764	212416	206.1728	−20.4595375061035	−15.9632005691528	−4.49633598327636
01698406	72272	194.22	−20.421007156372	−17.5319347381591	−2.88907194137573
01686685	163123	158.1134	−20.4010772705078	−17.0835590362548	−3.31751799583435
03831477	16867	182.209	−20.3915386199951	−14.6615343093872	−5.73000383377075
00264406	9430	164.1634	−20.3737277984619	−20.8172588348388	0.44352999329567
01848385	22947	154.1374	−20.2312488555908	−14.252947807312	−5.9783010482788
01666478	34493	234.9937	−20.1705150604248	−16.5286045074462	−3.64191102981567
05124992	156622	240.2054	−20.1524333953857	−14.8183116912841	−5.3341212272644
05046420	167907	190.52	−20.0034580230712	−17.6339092254638	−2.369549036026
00163863	10374	165.5761	−19.9736747741699	−18.0585403442382	−1.91513395309448
01556844	252063	175.1618	−19.9652576446533	−19.0271682739257	−0.93808901309967
05328516	202621	220.4425	−19.9621295928955	−18.4556083679199	−1.50652205944061
05502157	316460	169.0737	−19.8759479522705	−15.709394454956	−4.16655302047729
04791994	39807	160.086	−19.8585700988769	−16.719030380249	−3.13953900337219
00077612	24681	174.1098	−19.855224609375	−13.1103782653808	−6.74484682083129
01683924	52296	171.1734	−19.8534240722656	−15.9152507781982	−3.9381730556488
00157056	5395	211.1306	−19.8381252288818	−14.8757848739624	−4.96233987808227
01757822	227872	196.9851	−19.8202323913574	−16.5652732849121	−3.25496006011962
01565661	290947	195.1372	−19.8041515350341	−20.9308586120605	1.12670803070068
01652034	29194	214.2596	−19.7809505462646	−19.3727569580078	−0.408194005489349

ZINC A curated collection of commercial available chemical compounds; *VDW score* Van der Waal's interations; *ES score* Electrostatics

were not as dramatic as those of 100 μM, but were greater than the vehicle treatment. Furthermore, NCI-41356 (100 μM) triggered a significant apoptotic response in MDA-MB-231 compared to those of vehicle treatment (Supplementary Fig. 4a).

The addition of NCI-41356 to culture medium led to noticeable changes in the cell morphology of the breast cancer cells: the cells became less stellate, with lower proportions of lamellipodia, filopodia and trailing compared with those of vehicle treatment (Supplementary Fig. 4b). MDA-MB-231 cells express high levels of mesenchymal intermediate filament vimentin, which was down-regulated by NCI-41356 (100 μM) (Supplementary Fig. 4c, d). As these phenomena seemed to reflect the inhibitory effect of NCI-41356 on the migratory behaviour of the breast cancer cells, we determined the cell migratory

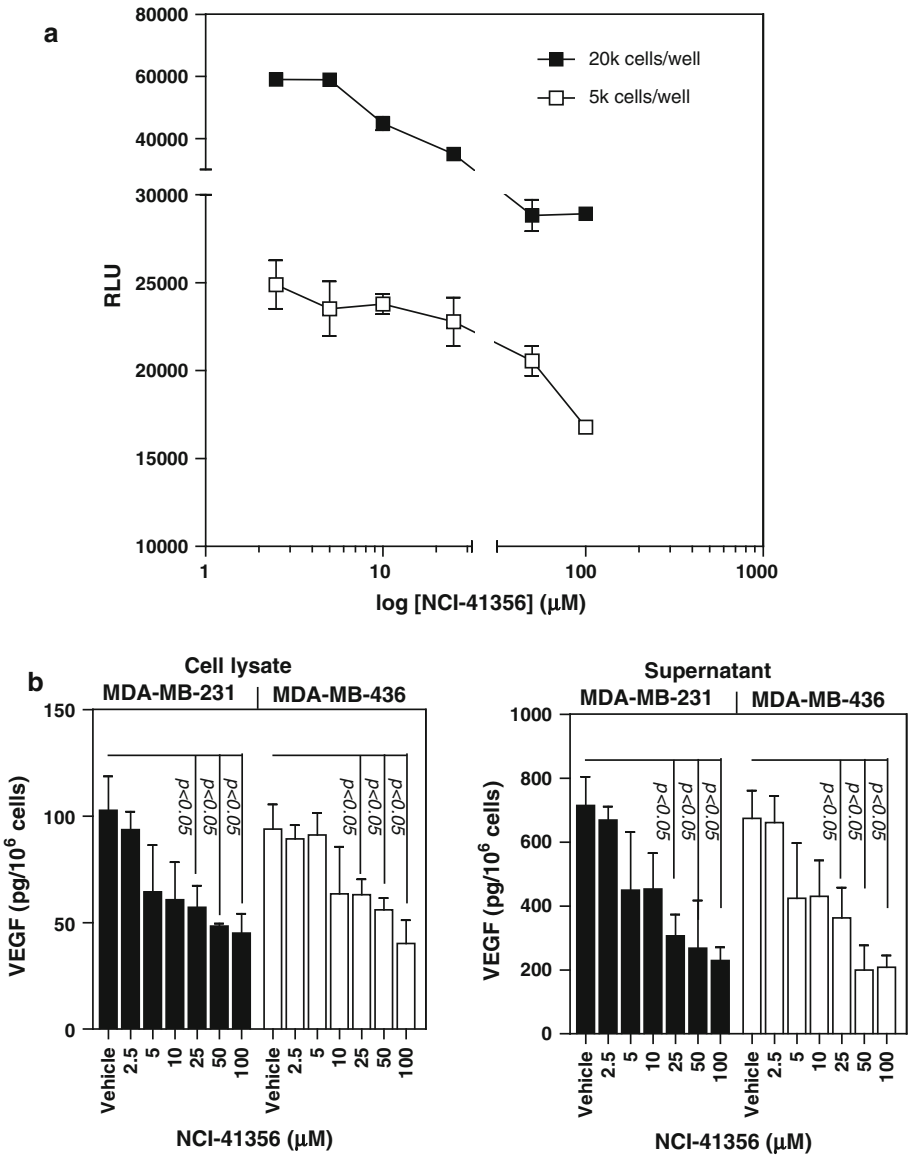

Fig. 2 NCI-41356 blocks the interaction between CRYAB and $VEGF_{165}$, and down-regulates $VEGF_{165}$ expression. **a** Concentration response curves to NCI-41356 in the two different cell densities (5 k/well or 20 k/wells) of U2OS cells expressing the PathHunter™ cell-based CRYAB/$VEGF_{165}$ interaction systems. Chemiluminescence is indicated as relative luminescence units (RLU). **b** $VEGF_{165}$ protein levels in both supernatants and cell lysates of breast cancer cells were measured by ELISA. The high expression $VEGF_{165}$ in breast cancer cells was attenuated by NCI-41356 in a dose-dependent manner. These experiments were repeated at least of three times, and the results are expressed as Mean ± SEM

ability of both breast cancer cells (MDA-MB-231 and MDA-MB-436) exposed to different concentrations of NCI-41356 (Fig. 3b). The highly motile MDA-MB-231 cells were not affected by the exposure to low doses (2.5–10 μM) of NCI-41356 with the similar migration as the vehicle control levels, while NCI-41356 treatments at a range of 25–50 μM led to noticeably reduced migratory speeds. The cells treated with 100 μM NCI-41356 showed by far the greatest migratory inhibition in the culture. MDA-MB-436 cells exhibited very similar change in migration in response to NCI-41356. Confluent MDA-MB-231 cells were wounded with a 2.5 mm scrape in one direction, and the closing movements of invading cell-fronts were photographed, followed by digital image analysis of the distances between the two wound edges (Fig. 3c).

Although TNBCs seem to be more likely to express CRYAB, many original breast cancer cell lines have been found to exhibit weaker or non-expression of CRYAB, such as parental MCF-7 [32]. To further validate whether the inhibitory effect of NCI-41356 on breast cancer cells is CRYAB-dependent, we treated MCF-7 cells with different doses of NCI-41356 followed by crystal violet assay. As shown in Supplementary Fig. 4e, the MCF-7 cells were largely insensitive to NCI-41356 in comparison with MDA-MB-231. Furthermore, NCI-41356 did not change VEGF expression/secretion in MCF-7 cells (Supplementary Fig. 4f). We also examined the effect of NCI-41356 on CRYAB expression breast cancer cells. NCI-41356 treatment (100 μM) did not alter CRYAB expression levels in both in vivo passaged MDA-MB-231 and MDA-MB-436 (Supplementary Fig. 5a).

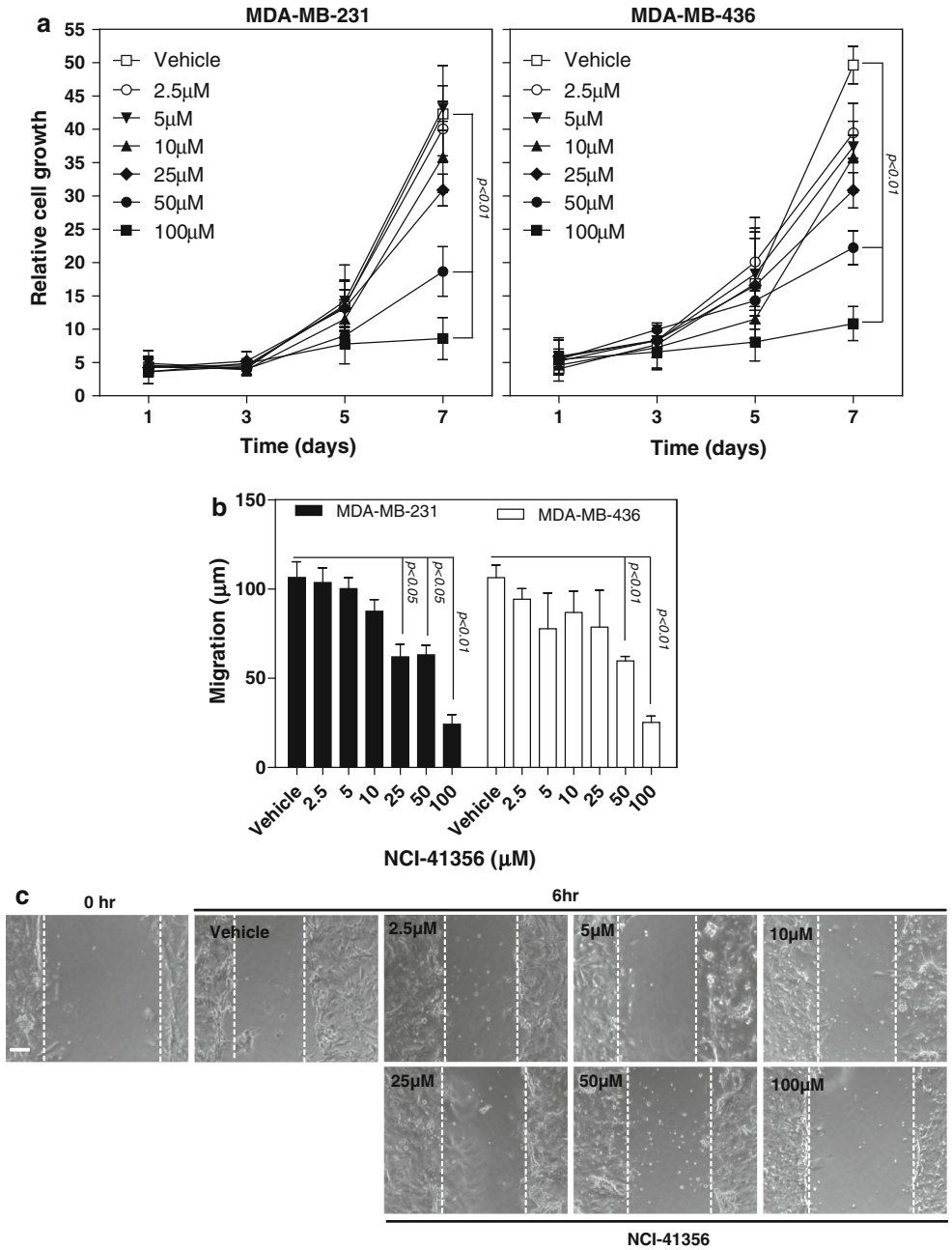

Fig. 3 NCI-41356 reduces tumourigenic progression of breast tumour. **a** Growth curves of breast cancer cell line treated with various concentrations of NCI-41356. At different times, the relative cell number of cells was analysed by crystal violet staining. The experiment was performed more than three independent times, and the results are expressed as Mean ± SEM. **b** The impact of NCI-41356 on the breast cancer cell migration was evaluated by the wound-healing assay. The experiment was performed more than three independent times, and the results are expressed as Mean ± SEM. **c** Confluent monolayers of MDA-MB-231 cells were wounded, and repair was monitored microscopically at time 0 and 6 h of incubation with the indicated doses of NCI-41356. Graph reflects the means of migratory distances of wounded. *Scale bar* 400 μm

Disruption of the interaction between CRYAB and $VEGF_{165}$ decreased breast cancer cell-induced in vitro angiogenic activity of endothelial cells

Tumour angiogenesis plays a crucial role in tumour development. Quiescent endothelial cells proliferate in response to various angiogenic growth factors including VEGF. Subsequently, the proliferating endothelial cells align into tubule-like structures which eventually form new functional blood vessels. Although endothelial cells express moderate levels of $VEGF_{165}$ protein [20], malignant breast cancer cells can produce over two orders of

magnitude greater levels of $VEGF_{165}$. NCI-41356 did not affect the proliferation of endothelial cell in the absence of breast cancer cell stimulation (Supplementary Fig. 5b). It is believed that tumour cells are the main source of VEGF stimulating angiogenic functions of endothelial cells within tumour microenvironment. We speculated that decrease of $VEGF_{165}$ production in breast cancer cells by NCI-41356 might affect cell proliferation and tubule formation of endothelial cells. To explore this possibility, we investigated the effects of NCI-41356 on tumour angiogenesis using our established in vitro co-culture system to stimulate endothelial cells by highly malignant MDA-MB-231 cells [33].

First, we determined the proliferation of human microvascular endothelial cells (HMECs) co-cultured with highly malignant MDA-MB-231 cells upon NCI-41356 treatment (Fig. 4a). HMECs stimulated by the MDA-MD-231 cells treated with various concentrations of NCI-41356 showed a significant decrease in cell proliferation in a dose-dependent manner compared with those of the vehicle treatment. Approximately, 50 % of HMEC proliferation was suppressed when the MDA-MB-231 cells were treated with 25 μM NCI-41356, and to near half level of the vehicle treatment at 100 μM, confirming that $VEGF_{165}$ secreted from MDA-MB-231 cells is a major source of VEGF. Second, the influence of MDA-MB-231 cell-associated NCI-41356 on angiogenic activity of HMEC was determined in order to further explore the potential inhibitory effect derived from the disruption of the interaction between CRYAB and $VEGF_{165}$ during tumour angiogenesis. We employed an in vitro tubule formation assay, in which MDA-MB-231 cell-stimulated HMECs are induced to form a network of capillary-like structures in 3D Matrigels. As shown in Fig. 4b, the dose-dependent effects of NCI-41356 on the MDA-MB-231 cells subsequently significantly affected HMEC in vitro tubule formation. Quantitative evaluation of tubule length revealed that the concentrations ≥10 μM of NCI-41356 decreased the length of the endothelial tubule structures by 38–67 % compared with those of the vehicle treatment (Fig. 4c).

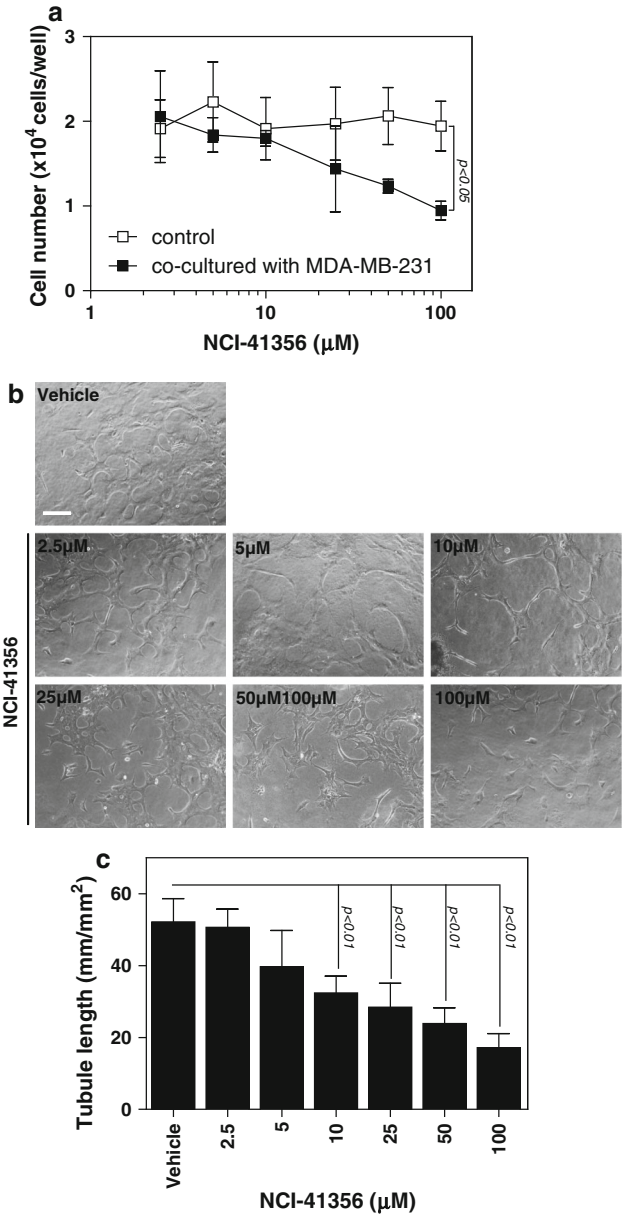

Fig. 4 NCI-41356 inhibits the MDA-MB-231 cell-stimulated angiogenic activities of endothelial cells. **a** Inhibitory effects of NCI-41356 on the MDA-MB-231 cell-induced proliferation of endothelial cells, determined by crystal violet staining. The experiment was performed more than three independent times, and the results are expressed as Mean ± SEM. **b** Representative photographs of microscopic field of in vitro tubule formation assay show a tubule-like network formation of endothelial cells between the two layers of Matrigels. *Scale bar* 400 μm. **c** Anti-angiogenic role of NCI-41356 on the MDA-MB-231 cell-stimulated in vitro angiogenesis, assessed by in vitro tubule formation assay. The tubule length (mm/mm^2) per microscopic field was quantified. The results are expressed as Mean ± SEM from at least three independent experiments

Disruption of the interaction between of CRYAB and $VEGF_{165}$ suppresses breast tumour growth in in vivo xenograft models

We evaluated the effects of NCI-41356 in inhibiting growth of human breast cancer xenograft in vivo. The highly malignant MDA-MD-231 cell line was intentionally selected for its high levels of in vitro response to NCI-41356. When the implanted tumour had reached a volume of ∼33 mm^3 by day 4 of tumour implant, the treatments were started (Fig. 5a). The growth curves of the two groups of mice that received NCI-41356 and the vehicle are shown in Fig. 5a. After the treatments, the tumour volume doubling time in the vehicle treatment group was 4.5 days, compared to 2.7 days in those of NCI-41356 treatment. In

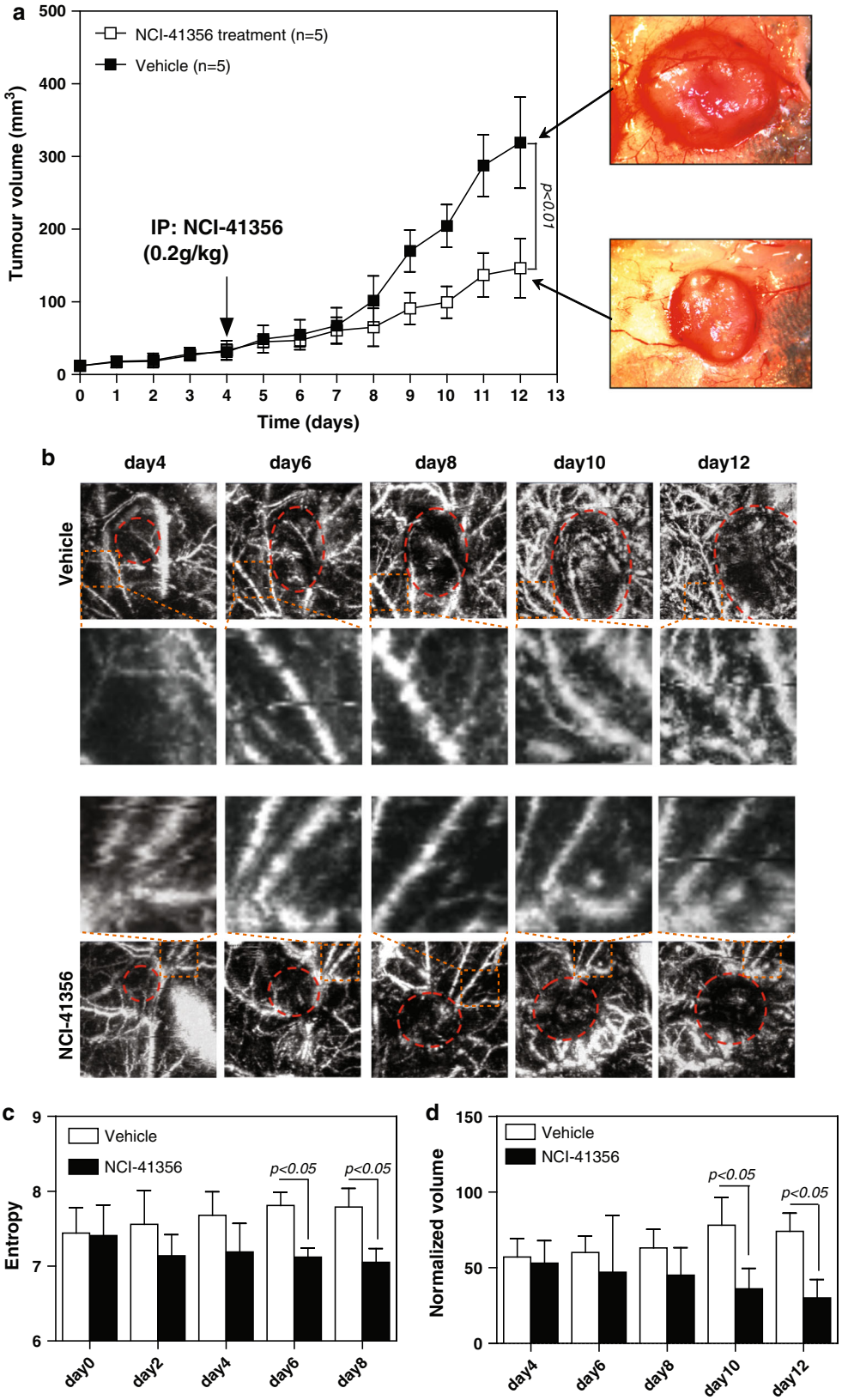

Fig. 5 Effects of NCI-41356 on the tumour growth and tumour vasculature development in a xenograft model. **a** Human breast cancer xenografts were established by subcutaneous injection of 1×10^5 MDA-MB-231 cells into the mammary fat pads of nude mice. The tumour volume was calculated from daily calliper measurements of the large (*a*) and smallest (*b*) diameters of each tumour using formula diameters of each tumour using formula $a \times b^2 \times 0.4$. Two tumour images represent the xenograft tumours IP injected with the vehicle (*top*) or NCI-41356 (*bottom*). **b** Serial photoacoustic (PA) imaging was performed on the same tumour inoculation site on day 4, 6, 8, 10 and 12 post tumour inoculations. Representative serial PA images of the xenografts i.p. injected with the vehicle (*first* and *second panels*) or NCI-41356 (*third* and *fourth panels*). **c** Entropy extraction for change in the vessel density over different time points as indicated. **d** Comparative analysis of normalized vessel volumes at different time points as indicated was performed. The experiment was repeated three times and each group contained 5 mice. The results are expressed as Mean ± SEM

50 % of mice treated with NCI-41356, the size of the subcutaneous tumour exceeded 150 mm^3 after 4 days of the treatment compared with 4.5 days of the vehicle treatment. In the vehicle treatment group, the tumour volume reached a maximum of $\sim$320 mm^3 by day 12 after tumour implantation. NCI-41356 treatment resulted in a significant twofold decrease in the growth of the xenograft tumours. CRYAB expression in xenograft tumours was observed by IHC in both mice treated with vehicle or NCI-41356 (Supplementary Fig. 5c). NCI-41356 treatment did not affect CRYAB expression by histological morphometric analysis (Supplementary Fig. 5d). We also observed that both VEGF and von Willebrand factor were decreased upon to NCI-41356 treatment, suggesting a strong role of NCI-41356 on down-regulation of VEGF and inhibition of tumour angiogenesis.

Disruption of the interaction between CRYAB and $VEGF_{165}$ reduced angiogenic responses in breast cancer xenograft models as monitored by serial photoacoustic (PA) imaging

Based on the striking in vitro and in vivo effects of NCI-41356 on breast cancer-induced angiogenesis, we performed noninvasively photoacoustic (PA) imaging to detect possible inhibitory effects of NCI-41356 on in vivo tumour vasculature development. Serial PA imaging was carried out on day 4, 6, 8, 10 and 12 after tumour implantation. In the vehicle-treated mice, the tumour vascular development manifested as gradually splitting large host blood vessels into smaller ones, while similar vascular changes were absent from those treated with NCI-41356 (the second panel in Fig. 5b). Using PA resolution and depth-section capacity, we acquired the kinetics of the vessel density changes surrounding tumour mass by statistically measuring the randomness of the texture of the input images using the Entropy method. In Fig. 5c, Entropy data clearly showed that NCI-41356 treatment caused a significant decrease in vessel density. In contrast, Entropy did not reveal a detectable change in vessel density in the vehicle treatment group. In order to confirm Entropy findings, we employed another PA image extraction analysis by normalizing vessel volume changes. As shown in Fig. 5d, NCI-41356 treatment resulted in a significant decrease in tumour vessel volume, while the vehicle treated mice exhibited a steep increased in the vessel volume.

Discussion

Work by Moyano et al. [16] indicated that CRYAB overexpression induced neoplastic-like transformation of human mammary epithelial cells. In vitro experiments clearly revealed that CRYAB overexpression promoted cell mobility and invasiveness of breast tumour cells. More strikingly, the authors demonstrated that a breast cancer xenograft arising from human mammary epithelial cells overexpressing CRYAB recapitulated aspects of human basal-like breast cancer, providing further evidence to support the rationale that CRYAB could be a therapeutic target for TNBC treatment. In vitro studies have established that targeting CRYAB using anti-sense or RNAi molecules causes cancer cells to be more sensitive to apoptotic inducers and anti-cancer drugs [22, 34].

It has been proposed that targeting CRYAB could lead to the degradation of a putative tumourigenic and/or metastatic proteins that may bind to CRYAB, such as $VEGF_{165}$ [35]. High $VEGF_{165}$ expression and its strong correlation with tumour growth and angiogenesis in breast cancer have been reported. There is considerable evidence from clinical and animal studies that VEGF receptors are highly expressed not only in vascular endothelial cells but also in various types of malignancies, in which they function in the autocrine and/or paracrine biological actions of cancer cells for survival in the tumour microenvironment independent of angiogenesis [36–38]. Apart from anti-angiogenesis strategy, aberrant highly activated autocrine/paracrine $VEGF_{165}$ signalling has become a critical target in the treatment of malignant breast cancer cells. Interestingly, it has been reported that CRYAB contains interactive sequences for $VEGF_{165}$, suggesting that CRYAB might chaperone and stabilize $VEGF_{165}$ [39]. Our recent data suggest for the first time that CRYAB might prevent the cellular stress-induced misfolded/unfolded $VEGF_{165}$ from proteolytic degradation, thereby maintaining internal autocrine (intracrine) VEGF signalling [20]. The intracrine VEGF signalling refers to endogenous VEGF and its receptors which internally transduce VEGF signalling without VEGF secretion and is crucial for cell homeostasis. Clinical studies have suggested the possible resistance development in anti-VEGF treatment for breast cancer patients [33]. We speculated that the intracrine VEGF signalling could act as primary intrinsic resistance for anti-VEGF therapy, while the unfolded protein response/CRYAB axle might be served as the acquired resistance [20]. It is logic to propose that down-regulation of intracellular VEGF signalling by targeting CRYAB might present a powerful addition to current anti-VEGF strategy in TNBC treatment. However, CRYAB is the most abundantly expressed small heat shock protein in cardiac muscles, reaching approximately 5 % of the total protein in cardiomyocytes and exerting strong protection of cardiomyocytes from many stresses [23]. Consistent with this notion, CRYAB knockout mice exhibit more vulnerability to ischaemic reperfusion injury while increased CRYAB expression in transgenic mice enhances functional recovery

of reperfusion injured hearts following global ischaemic stress [40]. The protective role of CRYAB has also been reported in damages to the CNV by modulating the immune system [24]. Hence, unwanted side effects may occur in patients with ischaemic heart diseases and/or stroke, seriously undermining the potential strategy of directly targeting CRYAB for TNBC treatment when systematically administering anti-CRYAB agents. In this context, the following question arose: could molecules (e.g. chemical compounds) that compete with $VEGF_{165}$ for binding to specific structures of CRYAB be an alternative approach to reduce the tumourigenic and metastatic activities of VEGF in addition to current anti-VEGF agents?

Over last decade, protein–protein interactions (PPIs) have emerged as attractive molecular targets for novel therapies, and the inhibition of PPIs relating to signalling cascades is particularly relevant to the discovery of novel therapeutic agents for cancer treatment [41]. Although the interfaces of PPIs are extensive, many studies showed that only 9.5 % of the interfacial amino acid residues (hotspots) significantly contribute to the stability of a complex and a ligand to hotspots can compete with the original partner resulting in disrupting function [42]. In this study, we described a three-step process to identify a small molecular inhibitor of the interaction between CRYAB and $VEGF_{165}$. Initially, our decoy peptidase corresponding to the sequences of the $VEGF_{165}$ interacting region of human CRYAB unravelled the 'hotspot' residues, which contribute to the interaction between CRYAB and $VEGF_{165}$. Second, we performed a virtual screen by the computational molecular docking based on a putative binding site from peptide binding to simulate the interaction of 139,735 small compounds (NCI Developmental Therapeutic Program). Third, we took the leading hit compounds forward to further function testing and found the compound NCI-41356 to possess the following important proof-of-concept cellular characteristics, albert within the micromolar range: (1) disruption of the interaction between CRYAB and $VEGF_{165}$ in a concentration-dependent manner, resulting in a substantial decrease in $VEGF_{165}$ expression and inhibitory effects on the proliferation and the invasion of TNBCs without affecting CRYAB levels; (2) decrease in in vitro angiogenic activities of endothelial cells co-cultured with MDA-MB-231 cells and (3) in the human breast cancer xenograft model, intraperitoneally applied NCI-41356 resulted in a marked decrease in the tumour growth and vasculature development.

The observed inhibitory effects of NCI-41356 on breast cancer in vitro and in vivo suggest that the interaction between CRYAB and $VEGF_{165}$ could present an important therapeutic target for TNBC. The disruption of the interaction between CRYAB and $VEGF_{165}$ can leave the cellular stress-induced $VEGF_{165}$ expression unprotected. This might result in not only a reduction in autocrine/paracrine VEGF signalling, but also an increase in the cytotoxicity of accumulated misfolded/unfolded $VEGF_{165}$ in cells. More interestingly, comparison of CRYAB interactive sequences revealed that the β3–β8–β9 surface appears to be a common surface for many growth factors including VEGF, NGF-β, FGF2 and Insulin [25]. In this study, we noticed that the concentration of NCI-41356 required to inhibit that breast cancer growth is higher than those needed to inhibit VEGF expression/secretion. We inferred that since the binding 'hotspots' of NCI-41356 located within the β3-β8-β9 common surface, NCI-41356 disrupting other growth factors might contribute to its inhibitory effects on breast cancer growth, which warrants further study. Regardless, the small molecular compound disrupting the interaction between CRYAB and $VEGF_{165}$ presented here will constitute useful tools to clarify the mechanisms of the CRYAB molecular chaperone functions in tumour development as well as a potential target for targeted therapy for TNBC in addition to current anti-angiogenesis regimens.

Acknowledgments This work was supported by Bankhead Coley Cancer Research Program (09BN-04) from the state Florida department of health in USA. Mr. Weilin Cai and Miss. Sioned Owen are acknowledged for assistance with proofreading.

Conflict of interest The authors declare that they have no competing interests.

References

1. Braden MA, Stankowski VR, Engel MJ, Onitilo AA (2013) Breast cancer biomarkers: risk assessment, diagnosis, prognosis, prediction of treatment efficacy and toxicity, and recurrence. Curr Pharm Des
2. Reis-Filho JS, Tutt AN (2008) Triple negative tumours: a critical review. Histopathology 52(1):108–118. doi:10.1111/j.1365-2559.2007.02889.x
3. Tischkowitz M, Brunet JS, Begin LR, Huntsman DG, Cheang MC, Akslen LA, Nielsen TO, Foulkes WD (2007) Use of immunohistochemical markers can refine prognosis in triple negative breast cancer. BMC Cancer 7:134. doi:10.1186/1471-2407-7-134
4. Gonzalez-Angulo AM, Timms KM, Liu S, Chen H, Litton JK, Potter J, Lanchbury JS, Stemke-Hale K, Hennessy BT, Arun BK, Hortobagyi GN, Do KA, Mills GB, Meric-Bernstam F (2011) Incidence and outcome of BRCA mutations in unselected patients with triple receptor-negative breast cancer. Clin Cancer Res 17(5):1082–1089. doi:10.1158/1078-0432.CCR-10-2560
5. Carey LA, Perou CM, Livasy CA, Dressler LG, Cowan D, Conway K, Karaca G, Troester MA, Tse CK, Edmiston S, Deming SL, Geradts J, Cheang MC, Nielsen TO, Moorman PG, Earp HS, Millikan RC (2006) Race, breast cancer subtypes, and survival in the Carolina Breast Cancer Study. JAMA 295(21):2492–2502. doi:10.1001/jama.295.21.2492
6. Bauer KR, Brown M, Cress RD, Parise CA, Caggiano V (2007) Descriptive analysis of estrogen receptor (ER)-negative,

progesterone receptor (PR)-negative, and HER2-negative invasive breast cancer, the so-called triple-negative phenotype: a population-based study from the California Cancer Registry. Cancer 109(9):1721–1728. doi:10.1002/cncr.22618
7. Millikan RC, Newman B, Tse CK, Moorman PG, Conway K, Dressler LG, Smith LV, Labbok MH, Geradts J, Bensen JT, Jackson S, Nyante S, Livasy C, Carey L, Earp HS, Perou CM (2008) Epidemiology of basal-like breast cancer. Breast Cancer Res Treat 109(1):123–139. doi:10.1007/s10549-007-9632-6
8. Kaplan HG, Malmgren JA, Atwood M (2009) T1N0 triple negative breast cancer: risk of recurrence and adjuvant chemotherapy. Breast J 15(5):454–460. doi:10.1111/j.1524-4741.2009.00789.x
9. Huo D, Ikpatt F, Khramtsov A, Dangou JM, Nanda R, Dignam J, Zhang B, Grushko T, Zhang C, Oluwasola O, Malaka D, Malami S, Odetunde A, Adeoye AO, Iyare F, Falusi A, Perou CM, Olopade OI (2009) Population differences in breast cancer: survey in indigenous African women reveals over-representation of triple-negative breast cancer. J Clin Oncol 27(27):4515–4521. doi:10.1200/JCO.2008.19.6873
10. Gravekamp C, Sypniewska R, Gauntt S, Tarango M, Price P, Reddick R (2004) Behavior of metastatic and nonmetastatic breast tumors in old mice. Exp Biol Med (Maywood) 229(7):665–675
11. Price DJ, Avraham S, Jiang S, Fu Y, Avraham HK (2004) Role of the aging vasculature and Erb B-2 signaling in epidermal growth factor-dependent intravasion of breast carcinoma cells. Cancer 101(1):198–205. doi:10.1002/cncr.20340
12. Xiong W, Li J, Chen L, Price RA, Freedman G, Ding M, Qin L, Yang J, Ma CM (2004) Optimization of combined electron and photon beams for breast cancer. Phys Med Biol 49(10):1973–1989
13. Kim LS, Huang S, Lu W, Lev DC, Price JE (2004) Vascular endothelial growth factor expression promotes the growth of breast cancer brain metastases in nude mice. Clin Exp Metastasis 21(2):107–118
14. Lee S, Chen TT, Barber CL, Jordan MC, Murdock J, Desai S, Ferrara N, Nagy A, Roos KP, Iruela-Arispe ML (2007) Autocrine VEGF signaling is required for vascular homeostasis. Cell 130(4):691–703. doi:10.1016/j.cell.2007.06.054
15. Samuel S, Fan F, Dang LH, Xia L, Gaur P, Ellis LM (2011) Intracrine vascular endothelial growth factor signaling in survival and chemoresistance of human colorectal cancer cells. Oncogene 30(10):1205–1212. doi:10.1038/onc.2010.496onc2010496
16. Moyano JV, Evans JR, Chen F, Lu M, Werner ME, Yehiely F, Diaz LK, Turbin D, Karaca G, Wiley E, Nielsen TO, Perou CM, Cryns VL (2006) AlphaB-crystallin is a novel oncoprotein that predicts poor clinical outcome in breast cancer. J Clin Invest 116(1):261–270. doi:10.1172/JCI25888
17. Sitterding SM, Wiseman WR, Schiller CL, Luan C, Chen F, Moyano JV, Watkin WG, Wiley EL, Cryns VL, Diaz LK (2008) AlphaB-crystallin: a novel marker of invasive basal-like and metaplastic breast carcinomas. Ann Diagn Pathol 12(1):33–40. doi:10.1016/j.anndiagpath.2007.02.004
18. Piatigorsky J (1984) Lens crystallins and their gene families. Cell 38(3):620–621
19. Iwaki T, Kume-Iwaki A, Goldman JE (1990) Cellular distribution of alpha B-crystallin in non-lenticular tissues. J Histochem Cytochem 38(1):31–39
20. Ruan Q, Han S, Jiang WG, Boulton ME, Chen ZJ, Law BK, Cai J (2011) alphaB-crystallin, an effector of unfolded protein response, confers anti-VEGF resistance to breast cancer via maintenance of intracrine VEGF in endothelial cells. Mol Cancer Res 9(12):1632–1643. doi:10.1158/1541-7786.MCR-11-0327
21. Acunzo J, Katsogiannou M, Rocchi P (2012) Small heat shock proteins HSP27 (HspB1), alphaB-crystallin (HspB5) and HSP22 (HspB8) as regulators of cell death. Int J Biochem Cell Biol 44(10):1622–1631. doi:10.1016/j.biocel.2012.04.002
22. Lee JS, Kim HY, Jeong NY, Lee SY, Yoon YG, Choi YH, Yan C, Chu IS, Koh H, Park HT, Yoo YH (2012) Expression of alphaB-crystallin overrides the anti-apoptotic activity of XIAP. Neuro Oncol 14(11):1332–1345. doi:10.1093/neuonc/nos247
23. Taylor RP, Benjamin IJ (2005) Small heat shock proteins: a new classification scheme in mammals. J Mol Cell Cardiol 38(3):433–444. doi:10.1016/j.yjmcc.2004.12.014
24. Ousman SS, Tomooka BH, van Noort JM, Wawrousek EF, O'Connor KC, Hafler DA, Sobel RA, Robinson WH, Steinman L (2007) Protective and therapeutic role for alphaB-crystallin in autoimmune demyelination. Nature 448(7152):474–479. doi:10.1038/nature05935
25. Ghosh JG, Shenoy AK Jr, Clark JI (2007) Interactions between important regulatory proteins and human alphaB crystallin. Biochemistry 46(21):6308–6317. doi:10.1021/bi700149h
26. Cai J, Jiang WG, Grant MB, Boulton M (2006) Pigment epithelium-derived factor inhibits angiogenesis via regulated intracellular proteolysis of vascular endothelial growth factor receptor 1. J Biol Chem 281(6):3604–3613. doi:10.1074/jbc.M507401200
27. Ruan Q, Xi L, Boye SL, Han S, Chen ZJ, Hauswirth WW, Lewin AS, Boulton ME, Law BK, Jiang WG, Jiang H, Cai J (2013) Development of an anti-angiogenic therapeutic model combining scAAV2-delivered siRNAs and noninvasive photoacoustic imaging of tumor vasculature development. Cancer Lett 332(1):120–129. doi:10.1016/j.canlet.2012.11.016
28. Yang JM, Maslov K, Yang HC, Zhou Q, Shung KK, Wang LV (2009) Photoacoustic endoscopy. Opt Lett 34(10):1591–1593
29. Bagneris C, Bateman OA, Naylor CE, Cronin N, Boelens WC, Keep NH, Slingsby C (2009) Crystal structures of alpha-crystallin domain dimers of alphaB-crystallin and Hsp20. J Mol Biol 392(5):1242–1252. doi:10.1016/j.jmb.2009.07.069
30. Derossi D, Joliot AH, Chassaing G, Prochiantz A (1994) The third helix of the Antennapedia homeodomain translocates through biological membranes. J Biol Chem 269(14):10444–10450
31. Jehle S, Rajagopal P, Bardiaux B, Markovic S, Kuhne R, Stout JR, Higman VA, Klevit RE, van Rossum BJ, Oschkinat H (2010) Solid-state NMR and SAXS studies provide a structural basis for the activation of alphaB-crystallin oligomers. Nat Struct Mol Biol 17(9):1037–1042. doi:10.1038/nsmb.1891
32. Chelouche-Lev D, Kluger HM, Berger AJ, Rimm DL, Price JE (2004) alphaB-crystallin as a marker of lymph node involvement in breast carcinoma. Cancer 100(12):2543–2548. doi:10.1002/cncr.20304
33. Bergers G, Hanahan D (2008) Modes of resistance to anti-angiogenic therapy. Nat Rev Cancer 8(8):592–603. doi:10.1038/nrc2442
34. Kamradt MC, Lu M, Werner ME, Kwan T, Chen F, Strohecker A, Oshita S, Wilkinson JC, Yu C, Oliver PG, Duckett CS, Buchsbaum DJ, LoBuglio AF, Jordan VC, Cryns VL (2005) The small heat shock protein alpha B-crystallin is a novel inhibitor of TRAIL-induced apoptosis that suppresses the activation of caspase-3. J Biol Chem 280(12):11059–11066. doi:10.1074/jbc.M413382200
35. van de Schootbrugge C, Bussink J, Span PN, Sweep FC, Grenman R, Stegeman H, Pruijn GJ, Kaanders JH, Boelens WC (2013) alphaB-crystallin stimulates VEGF secretion and tumor cell migration and correlates with enhanced distant metastasis in head and neck squamous cell carcinoma. BMC Cancer 13:128. doi:10.1186/1471-2407-13-128
36. Duffy AM, Bouchier-Hayes DJ, Harmey JH (2000) Vascular endothelial growth factor (VEGF) and its role in non-endothelial cells: autocrine signalling by VEGF. Landes Bioscience. http://www.ncbi.nlm.nih.gov/books/NBK6482/

37. Masood R, Cai J, Zheng T, Smith DL, Hinton DR, Gill PS (2001) Vascular endothelial growth factor (VEGF) is an autocrine growth factor for VEGF receptor-positive human tumors. Blood 98(6):1904–1913
38. Mercurio AM, Lipscomb EA, Bachelder RE (2005) Non-angiogenic functions of VEGF in breast cancer. J Mammary Gland Biol Neoplasia 10(4):283–290. doi:10.1007/s10911-006-9001-9
39. Kerr BA, Byzova TV (2011) alphaB-crystallin: a novel VEGF chaperone. Blood 115(16):3181–3183. doi:10.1182/blood-2010-01-262766
40. Morrison LE, Whittaker RJ, Klepper RE, Wawrousek EF, Glembotski CC (2004) Roles for alphaB-crystallin and HSPB2 in protecting the myocardium from ischemia-reperfusion-induced damage in a KO mouse model. Am J Physiol Heart Circ Physiol 286(3):H847–H855. doi:10.1152/ajpheart.00715.2003
41. White AW, Westwell AD, Brahemi G (2008) Protein–protein interactions as targets for small-molecule therapeutics in cancer. Expert Rev Mol Med 10:e8. doi:10.1017/S1462399408000641
42. Moreira IS, Fernandes PA, Ramos MJ (2007) Hot spots—a review of the protein–protein interface determinant amino-acid residues. Proteins 68(4):803–812. doi:10.1002/prot.21396